New Journal of Physics
The open-access journal for physics

Realizing analogues of color superconductivity with ultracold alkali atoms

K M O'Hara
Department of Physics, Pennsylvania State University, University Park, PA 16802, USA
E-mail: kohara@phys.psu.edu

New Journal of Physics **13** (2011) 065011 (23pp)
Received 23 February 2011
Published 20 June 2011
Online at http://www.njp.org/
doi:10.1088/1367-2630/13/6/065011

Abstract. A degenerate three-component Fermi gas of atoms with identical attractive interactions is expected to exhibit superfluidity and magnetic order at low temperature and, for sufficiently strong pairwise interactions, become a Fermi liquid of weakly interacting trimers. The phase diagram of this system is analogous to that of quark matter at low temperature, motivating strong interest in its investigation. We describe how a three-component gas below the superfluid critical temperature can be prepared in an optical lattice. To realize an SU(3)-symmetric system, we show how pairwise interactions in the three-component atomic system can be made equal by applying radiofrequency and microwave radiation. Finally, motivated by the aim to make more accurate models of quark matter, which have color, flavor and spin degrees of freedom, we discuss how an atomic system with SU(2) $\otimes$ SU(3) symmetry can be achieved by confining a three-component Fermi gas in the p-orbital band of an optical lattice potential.

Contents

1. Introduction **2**
2. Multi-component alkali gases **3**
3. Superfluidity, magnetism and trimer formation in a three-component Fermi gas **4**
3.1. Superfluidity in a three-component Fermi gas 5
3.2. Magnetism in a three-component Fermi gas 6
3.3. Trimer formation of strongly interacting fermions in an optical lattice 6
3.4. Analogies to color superconductivity and the chromodynamics (QCD) phase diagram 7
4. Achieving color superfluidity in an optical lattice **8**
5. Realizing SU(3)-invariant interactions **13**
6. Analogues of color superconductivity with color and spin **18**
Acknowledgments **22**
References **22**

1. Introduction

At densities present inside neutron stars, matter may be compressed to the point where quarks are no longer confined in hadrons but instead form a degenerate Fermi liquid. Due to attractive interactions between quarks of unlike color, Cooper pairing occurs near the Fermi surface. In forming Cooper pairs, the color gauge symmetry SU(3) is spontaneously broken. While this color superconducting phase is relatively well understood at extremely high quark density (where interactions are weak due to asymptotic freedom), the nature of the color superconducting phase at intermediate densities relevant to neutron stars is unknown [1]. Furthermore, the crossover between quark matter and hadronic matter that occurs at still lower densities is poorly understood [1]. This low-temperature, high-density region of the phase diagram of quantum chromodynamics (QCD) is not accessible to terrestrial experiments and cannot be calculated with lattice QCD due to the fermion sign problem [1].

A degenerate three-component Fermi gas of atoms provides an experimentally accessible system in which to explore similar phenomena. A three-component Fermi gas with identical attractive pairwise interactions, for example, becomes superfluid at low temperature, breaking the global SU(3) symmetry of the original Hamiltonian [2–11]. The symmetry breaking pattern is SU(3) → SU(2) [4, 5]. This parallels the symmetry breaking pattern [SU(3)] → [SU(2)] in two-flavor color superconductivity—a competitive candidate model of color superconductivity at intermediate densities. Here, the brackets denote gauge (rather than global) symmetries. In addition to superfluidity, a three-component Fermi gas also exhibits spontaneous magnetization driven by pairing [5, 12, 13]. The Ginzburg–Landau (GL) free energy for a three-component Fermi gas therefore contains two coupled order parameters for superfluidity and magnetization, respectively [11, 12]. The structure of the GL free energy is identical to that of dense quark matter where the two coupled order parameters in this case describe the quark–quark condensate and chiral condensate [11]. The phase diagram of a three-component Fermi gas thus shares many similarities with the phase diagram of QCD. Indeed, a three-component Fermi gas confined in a lattice also has a transition that parallels the deconfinement–hadronization transition in

QCD [13, 14]. In the limit of strong coupling, the three-component Fermi gas becomes a Fermi liquid of weakly interacting three-body cluster states. Since many parameters, including density, interaction strength and population imbalance, can be independently controlled in ultracold atomic gases, the entire phase diagram can be explored systematically.

In this paper, we review the properties of three-component Fermi gases. We describe how, in spite of significant loss rates due to three-body recombination, superfluidity can be achieved by confining ^{6}Li atoms at low density in a large-period optical lattice. We then discuss how scattering properties can be tuned, by applying radiofrequency (RF) and microwave (MW) fields, to achieve nearly perfect SU(3) symmetry in the atomic system. Finally, motivated by the aim to make more accurate models of quark matter, which have color, flavor and spin degrees of freedom, we discuss how an atomic system with SU(2) $\otimes$ SU(3) symmetry can be realized by confining a three-component Fermi gas in the p-orbital band of an optical lattice.

2. Multi-component alkali gases

Atomic alkali gases containing more than two components can be attained since the total angular momentum $\mathbf{F}$ (which is the sum of the nuclear $\mathbf{I}$ and electron $\mathbf{S}$ spin) allows for $2F+1$ degenerate internal states in zero magnetic field. For atoms with $I > 0$, F can be greater than $1/2$. Furthermore, in the presence of a large magnetic field (i.e. the Paschen–Back limit)[1], the good quantum numbers are m_S and m_I and there are two multiplets of $(2I+1)$ closely spaced levels with a given multiplet having the same electron spin projection, either $m_S = \pm 1/2$ (see, for example, figure 1(a)). The pairwise interactions between atoms in a given multiplet are nearly identical since the molecular interaction potential is independent of the nuclear spin. At ultralow temperatures, the interactions are purely s-wave and parameterized by an s-wave scattering length a. For pairwise interactions among states within a multiplet, the atoms interact predominantly via the triplet molecular potential and accordingly the pairwise scattering lengths are all given approximately by the triplet scattering length a_t.

In this paper, we will consider a gas of fermionic ^{6}Li atoms, which has a nuclear spin $I = 1$. The energies of the Zeeman states in ^{6}Li are shown in figure 1(a) as a function of magnetic field B. For $B \gg 100$ G, the states separate into multiplets with $|m_s, m_i\rangle = |-\frac{1}{2}, \{1, 0, -1\}\rangle$ in the lower-energy multiplet and $|m_s, m_i\rangle = |\frac{1}{2}, \{-1, 0, 1\}\rangle$ in the higher-energy multiplet. We label these states $|1\rangle$–$|6\rangle$ in order of increasing energy. We will consider a three-color Fermi gas comprised of atoms in states $|1\rangle$–$|3\rangle$. The scattering lengths for the three possible pairwise interactions between these states (a_{12}, a_{23} and a_{13}) are shown in figure 1(b). The scattering lengths a_{12}, a_{23} and a_{13} each exhibit a Feshbach resonance where the scattering length diverges at respective fields of 834, 811 and 690 G. Of central relevance to this paper, however, is the fact that at high field, the scattering lengths all asymptote to the triplet scattering length for ^{6}Li, $a_t = -2140\, a_0$.[2] Thus, in the limit of large fields, the pairwise interactions in the gas are attractive and of approximately equal magnitude. At a field of 2000 G, for example, the three scattering lengths are all within 2% of their average [15]. In section 5, we will show how the difference between the scattering lengths can be reduced even further if RF radiation is applied to dress the internal states of the atoms.

[1] In the Paschen–Back limit, the interaction energy of the field with the electron's magnetic moment greatly exceeds the hyperfine interaction.

[2] The anomalously large magnitude of a_t is due to a zero-energy resonance in the triplet molecular potential.

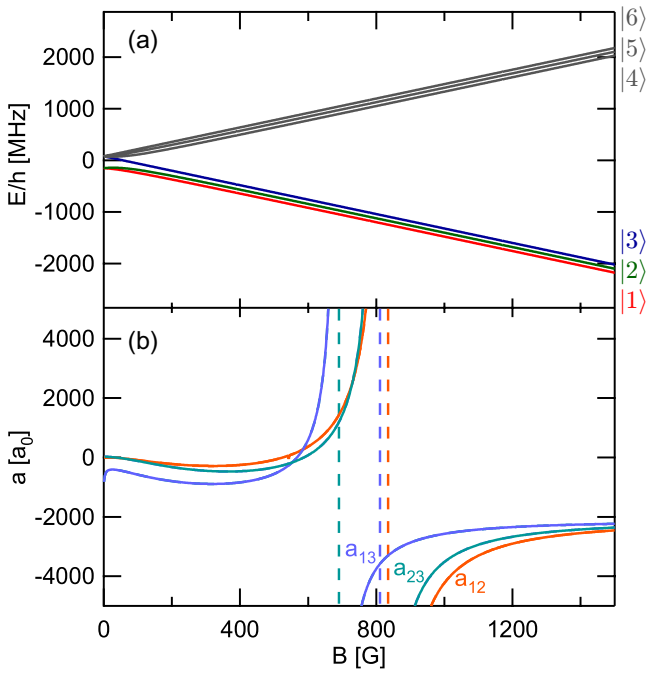

Figure 1. (a) Zeeman state energies of ^{6}Li atoms as a function of magnetic field B. The three lowest-energy states (labeled $|1\rangle$, $|2\rangle$ and $|3\rangle$) are the three internal states of ^{6}Li that will represent the color degree of freedom. For $B \gtrsim 200\,\mathrm{G}$, the z-projections of the electron and nuclear spin (m_s and m_i, respectively) are good quantum numbers and $|1\rangle \approx |-\frac{1}{2}, 1\rangle$, $|2\rangle \approx |-\frac{1}{2}, 0\rangle$ and $|3\rangle \approx |-\frac{1}{2}, -1\rangle$ in the $|m_\mathrm{s}, m_\mathrm{i}\rangle$-basis. (b) The s-wave scattering length for each of the three possible pairwise interactions between states $|1\rangle$–$|3\rangle$ as a function of B [15]. Magnetically tunable Feshbach resonances occur at $B = 690$, 811 and 834 G. For $B > 1000\,\mathrm{G}$, all three scattering lengths asymptote to the triplet scattering length $a_\mathrm{t} = -2140 a_0$.

3. Superfluidity, magnetism and trimer formation in a three-component Fermi gas

In this section, we will review the recent theoretical predictions regarding the phase diagram of a three-component Fermi gas with attractive interactions. We will then highlight several striking analogies that can be drawn between superfluidity in the atomic gas and color superconductivity in quark matter and also between the phase diagram of QCD and that of the atomic system.

The Hamiltonian for a homogeneous three-component Fermi gas in a volume V with identical scattering lengths a_t is given by

$$H = \sum_{k,\alpha} \left(\frac{\hbar^2 k^2}{2m} - \mu_\alpha \right) \psi^\dagger_{\sigma,\mathbf{k}} \psi_{\sigma,\mathbf{k}} + \frac{g}{2V} \sum_{\alpha,\beta} \sum_{\mathbf{k},\mathbf{k}',\mathbf{q}} \psi^\dagger_{\beta,\mathbf{k}'-\mathbf{q}} \psi^\dagger_{\alpha,\mathbf{k}+\mathbf{q}} \psi_{\alpha,\mathbf{k}} \psi_{\beta,\mathbf{k}'}, \tag{1}$$

where $\psi^\dagger_{\alpha,\mathbf{k}}$ is the creation operator of a particle in state $\alpha = 1, 2, 3$ with momentum $\hbar\mathbf{k}$, μ_α is the chemical potential for each color, and $g = \frac{4\pi\hbar^2 a_\mathrm{t}}{m}$ is the interaction strength. This Hamiltonian

is invariant under global SU(3) transformations of the three component field operator ψ (i.e. $\psi_\sigma \to U_{\sigma',\sigma}\psi_\sigma$ where $U \in \mathrm{SU}(3)$) as well as a global U(1) transformation of the overall phase.

3.1. Superfluidity in a three-component Fermi gas

For attractive contact interactions, fermionic atoms in different internal states form s-wave Cooper pairs at low temperature, giving rise to a pairing mean field $\Delta_{\alpha\beta} \propto \sum_{\mathbf{k}} \langle \psi_{\mathbf{k}\alpha}\psi_{-\mathbf{k}\beta}\rangle$ with nonzero components. The symmetry breaking pattern for the superfluid transition can be determined from group theoretical considerations, as was first done in [4]. Since pairing is in the s-wave channel, the 3×3 matrix $\Delta_{\alpha\beta}$ is antisymmetric and therefore has three independent complex components (e.g. Δ_{12}, Δ_{23} and Δ_{13}). Thus, $\Delta_{\alpha\beta}$ transforms according to a three-dimensional (3D) representation. Using the decomposition $3 \otimes 3 = \bar{3} \oplus 6$ for the SU(3) group (where 3 denotes the irreducible representation under which ψ_α is transformed and $\bar{3}$ is the complex conjugate representation of 3), we see that $\Delta_{\alpha\beta}$ transforms under the complex conjugate representation $\bar{3}$. This indicates that $\Delta_{\alpha\beta}$ transforms nontrivially under SU(3) and takes on different values depending on the global gauge of the fermions [14]. Thus, Cooper pairing spontaneously breaks the SU(3) symmetry of the model Hamiltonian equation (1). This is in stark contrast to the situation realized in a two-component Fermi gas symmetric under global $\mathrm{U}(1) \otimes \mathrm{SU}(2)$ transformations. Here, the antisymmetric 2×2 matrix has a single independent complex component and therefore transforms as a scalar under SU(2) (consistent with the decomposition $2 \otimes 2 = 1 \oplus 3$ for the SU(2) group). Thus, in the two-component case, Cooper pairing does not break SU(2) symmetry. Rather, the symmetry breaking pattern is $\mathrm{SU}(2) \otimes \mathrm{U}(1) \to \mathrm{SU}(2)$. We refer to superfluidity in a three-component Fermi gas where the SU(3) symmetry is spontaneously broken as 'color' superfluidity to distinguish it from the superfluid phase in a two-component Fermi gas (or a three-component Fermi gas without SU(3) symmetry), where only the U(1) symmetry is spontaneously broken.

To determine the symmetry breaking pattern in an $\mathrm{SU}(3) \otimes \mathrm{U}(1)$ symmetric three-component Fermi gas, we follow [11, 14] and consider the fermionic pairing order parameter,

$$\Delta_\alpha \propto \frac{1}{2}\epsilon_{\alpha\beta\gamma}\langle \psi_\beta \psi_\gamma \rangle = \begin{pmatrix} \Delta_{23} \\ -\Delta_{13} \\ \Delta_{12} \end{pmatrix}, \tag{2}$$

where $\epsilon_{\alpha\beta\gamma}$ is the total antisymmetric tensor. It is straightforward to show that this pairing order parameter transforms under the complex conjugate representation $\bar{3}$ such that $\Delta_\alpha \to U^*_{\alpha\beta}\Delta_\beta$ when $\psi_\alpha \to U_{\alpha\beta}\psi_\beta$ for $U \in \mathrm{SU}(3)$ [11]. Since U^* is also a unitary matrix, it is always possible to preserve the inner product $\sum_\alpha |\Delta_\alpha|^2 = \Delta_0$ but transform to a gauge where $\Delta = (0, 0, \Delta_0)$. In this gauge, only two components are paired with one component left unpaired and the unbroken symmetries are made explicit. The system is invariant under SU(2) transformations in the subspace of the two paired components and under U(1) transformations of the global phase of the unpaired component. Thus, the symmetry breaking pattern is $\mathrm{SU}(3) \otimes \mathrm{U}(1) \to \mathrm{SU}(2) \otimes \mathrm{U}(1)$. Spontaneous symmetry breaking in this system yields five broken generators and one expects five corresponding Nambu–Goldstone modes. Again, this can be contrasted with the situation in a superfluid two-component Fermi gas where a single generator is broken, giving rise to a single Nambu–Goldstone mode—the Anderson–Bogoliubov mode.

In the gauge where only two-components of the Fermi gas are paired, it is straightforward to apply a mean-field BCS theory to find the superfluid critical temperature T_c. This was first done by Modawi and Leggett [2], who found that

$$\frac{T_c}{T_F} = \frac{8\,e^{\gamma-2}}{\pi} \exp[-\pi/(2k_F\,|a_t|)], \tag{3}$$

where T_F is the Fermi temperature, k_F is the Fermi wavenumber and γ is Euler's constant. Assuming $a_t = -2140a_0$ and the density of each spin state is 3×10^{12} atoms cm^{-3}, the critical temperature $T_c = 0.05\,T_F$. At higher densities, the gas enters the strong coupling regime for which $k_F\,a_t \gtrsim 1$ and BCS theory is invalid. In the unitarity limit ($k_F\,a_t \gg 1$), one expects T_c to be a universal fraction of T_F. For a two-component Fermi gas, $T_c \simeq 0.15\,T_F$ in the unitarity limit and one might expect a comparable T_c for a three-component Fermi gas in the strong coupling limit. While temperatures $T < 0.05\,T_F$ at densities $\geqslant 3 \times 10^{12}$ atoms cm^{-3} have been experimentally achieved in a two-component Fermi gas, large loss rates in three-component Fermi gases due to three-body recombination have precluded the simultaneous achievement of low temperatures and high densities. In section 4, we describe how superfluidity in a three-component Fermi gas can be achieved by confining a low-density gas in an optical lattice potential.

3.2. Magnetism in a three-component Fermi gas

In addition to superfluidity, a three-component gas also exhibits spontaneous magnetic ordering (i.e. population imbalance) [5, 12] characterized by a secondary order parameter $\phi \equiv \frac{N_1}{V} - \frac{N}{3V}$ [11]. Here, N_1 is the number of particles in state $|1\rangle$ and $N = 2N_1 + N_3$ is the total number of particles in the gauge where states $|1\rangle$ and $|2\rangle$ pair and state $|3\rangle$ is unpaired. Physically, population imbalance occurs since the energy of the system can be minimized for a fixed total number of atoms by transferring population from the unpaired state $|3\rangle$ into the pairing states $|1\rangle$ and $|2\rangle$ where their energy is reduced by the condensation energy. Magnetization is observed in mean-field Bardeen, Cooper and Schrieffer (BCS) theory by fixing the total number of atoms but allowing the number of atoms in each state to vary. Since superfluidity drives magnetization in the three-component system, $\phi > 0$ only when $\Delta > 0$ [5, 11, 12]. Mean-field theory indicates that the fractional population of one of the paired states grows from 33% in the limit of weak interactions to 41% at unitarity (where $a \to \infty$) to 50% in the BEC limit where dimer molecules form [5, 11]. In an experimental system where the population in each state is individually conserved, population imbalance manifests itself as the formation of domains where each domain contains an equal number of paired species but a smaller number of unpaired species. The species that pair in different domains are not the same and therefore the three-component order parameter Δ points in different directions for different domains.

3.3. Trimer formation of strongly interacting fermions in an optical lattice

The phenomena of color superfluidity and magnetic ordering also occur if the three-component Fermi gas is confined in the lowest band of a three-dimensional (3D) cubic lattice potential. However, in this case, Rapp *et al* [13] showed that, in the limit of strong interactions, the ground state becomes a Fermi gas of repulsively interacting three-body clusters (i.e. trimers).

The Hamiltonian for an SU(3) symmetric three-component Fermi gas confined in the lowest Bloch band of a 3D cubic lattice is given by

$$H_{\mathrm{H}} = -t \sum_{\langle ij\rangle,\alpha} \left(c^{\dagger}_{i,\alpha} c_{j,\alpha} + c^{\dagger}_{j,\alpha} c_{i,\alpha} \right) + \frac{U}{2} \sum_{i} \sum_{\alpha\neq\beta} n_{i,\alpha} n_{i,\beta}, \tag{4}$$

where $c^{\dagger}_{i,\alpha}$ is a fermionic creation operator for a particle on site i in state α, t is the tunneling matrix element for nearest neighbor hopping, $\langle ij\rangle$ indicates that the sum is over nearest neighbors, U is the strength of the on-site interaction, and $n_{i,\alpha} = c^{\dagger}_{i,\alpha} c_{i,\alpha}$. Note that only fermions in different internal states interact and $U < 0$ for attractive interactions. For weak interactions, $|U|/t \ll 1$, the ground state is a color superfluid that spontaneously breaks SU(3) symmetry [3, 4]. However, in the limit of strong interactions, $|U|/t \ll 1$, the tunneling term in equation (4) can be neglected and the on-site interaction term is minimized when three atoms in different internal states occupy the same lattice site [13]. Thus, the ground state in this limit consists of three-atom trimers localized on individual sites of the lattice. If the hopping term is introduced as a perturbation, it allows, in second order, the trimers to reduce their kinetic energy by an amount $\sim \frac{t^2}{|U|}$ by the virtual tunneling of individual atoms to adjacent unoccupied lattice sites [13]. However, virtual tunneling to an adjacent site is forbidden by the exclusion principle if it is occupied by another trimer. Thus, only isolated trimers can fully reduce their kinetic energy by virtual fluctuations, giving rise to an effective repulsion between the trimers [13]. To third order in t, an entire trimer can tunnel to an adjacent site with an effective tunneling matrix element $t_{\mathrm{tri}} = \frac{t^3}{|U|^2}$ [13]. Thus, the ground state in this limit is a gas of trimers with large effective mass and weak repulsive interactions. Note that this phase is invariant under global SU(3) transformations since the three-body color wavefunction of a trimer must be an (antisymmetric) color-singlet state. Therefore, a quantum phase transition must separate the color superfluid phase and the trimer phase since they have different symmetries [13].

3.4. Analogies to color superconductivity and the chromodynamics (QCD) phase diagram

There are several striking analogies between the three-component Fermi gas described above and matter at densities found inside neutron stars. In neutron stars, nuclei may be compressed to the point that quarks become deconfined from hadrons and form a degenerate Fermi liquid. At sufficiently high density, the Fermi liquid becomes weakly interacting as a consequence of asymptotic freedom. In this weak coupling limit, the quark–quark interaction is attractive for the color anti-triplet configuration [16]. Thus, in the low-temperature high-density limit, one expects quark matter to be a degenerate liquid of quarks with Cooper pairing between quarks of unlike color. Since pairs of quarks cannot be color singlets, the quark–quark condensate by necessity breaks the SU(3) color gauge symmetry. By an essentially identical argument, we showed in section 3.1 that the SU(3) symmetry in a three-component Fermi gas is broken by Cooper pairing. In fact, the symmetry breaking pattern in two-flavor color superconductivity is SU(3) → SU(2). A notable difference between the atomic gas and quark matter is that a *global* SU(3) symmetry is broken in the former whereas a *gauge* SU(3) symmetry is broken in the latter.

The difference between global and gauge SU(3) symmetries notwithstanding, a three-component Fermi gas can provide an analogue of dense quark matter that is experimentally accessible. For example, Ozawa and Baym [11] recently showed that the GL free energy for a three-component Fermi gas is identical in structure to that for quark matter. In the GL free

energy for dense quark matter, two coupled order parameters appear: one for quark–quark condensation and a second for chiral symmetry breaking [17, 18]. In the GL free energy for a three-component Fermi gas, there is a one-to-one correspondence between these two order parameters and the order parameters for pairing and population imbalance, respectively. While the structure of the GL free energy is identical to fourth order in the order parameters, the coefficients of two terms in the order parameter expansion can differ in sign [11]. Physically, the difference between the two systems arises from the fact that population imbalance in a three-component Fermi gas is *only* driven by pairing, whereas chiral symmetry breaking in dense quark matter can occur even in the absence of quark–quark pairing [11].

Three-component Fermi gases also offer the possibility of studying an analogue of the QCD deconfinement–hadronization transition. As discussed in section 3.3, Rapp *et al* [13] have shown that Cooper pairing in a three-component Fermi gas should eventually give way to the formation of a weakly interacting gas of bound three-body cluster states. This is similar to the formation of baryons from quark matter as the density of quarks is reduced. Thus, the phase diagram for a three-component Fermi gas with attractive identical interactions closely mimics the conjectured phase diagram of QCD. A color superconducting ground state exists in the limit of weak interactions (high quark chemical potential) and gives way to the formation of color singlet trimers (baryons) in the limit of strong interactions (low quark chemical potential).

4. Achieving color superfluidity in an optical lattice

In section 3.1, we noted that the critical temperature T_c in a homogeneous gas can be made as large as $0.05T_F$–$0.15T_F$ for $a_t = -2140\,a_0$ and a density in each spin state $n_\alpha \gtrsim 3 \times 10^{12}\,\mathrm{cm}^{-3}$. However, degenerate three-component Fermi gases at densities this large are difficult to achieve due to a large rate of inelastic three-body recombination events [19]. In a three-body recombination event, the collision of three atoms results in the formation of a tightly bound molecular dimer and a free atom. The binding energy released in forming the dimer is far greater than the depth of the confining potential and both the atom and the molecule are lost. Three-body recombination is not a significant problem in two-component Fermi gases as the event rate is suppressed by the exclusion principle since two of the three fermions involved in the s-wave collision must be identical [20]. However, this suppression mechanism does not exist in a three-component Fermi gas and the recombination event rate can be quite high [19]. The density of atoms in a homogeneous system decreases according to $\dot{n}_\alpha = -K_3 n_1 n_2 n_3$, where K_3 is the recombination rate constant.

For three fermions interacting via short-range potentials, all three-body observables, including the recombination rate constant K_3, can be expressed in terms of universal functions of the scattering length a and a complex valued three-body parameter $\tilde{\kappa} = \kappa_* + \mathrm{i}\,\eta_*$ (as long as the scattering length is large compared with the characteristic range of the interaction potential) [21]. The recombination rate is given by $K_3 = C(\tilde{\kappa}, a)\,\hbar\,a^4/m$, where $C(\tilde{\kappa}, a)$ is a universal function that is log-periodic in a [21]. The three-body parameter $\tilde{\kappa}$ has been determined experimentally for the ^{6}Li system in the magnetic field regime of interest for color superfluidity [19]. At a field of 2000 G where $a_t \simeq -2222 a_0$, the recombination rate constant $K_3 = 5.8^{+2.1}_{-3.6} \times 10^{-22}\,\mathrm{cm}^6\,\mathrm{s}^{-1}$. Thus, for a three-component gas with equal densities $n = n_{1,2,3} = 3 \times 10^{12}\,\mathrm{cm}^{-3}$, the fractional atom loss rate $\dot{n}/n = -K_3 n^2 \simeq -5220\,\mathrm{s}^{-1}$, suggesting that the density is reduced by $1/e$ in only 190 μs. Since the fractional atom loss rate is proportional to the square of the density, the loss rate can be dramatically reduced by significantly lowering

the density. However, the BCS critical temperature (equation (3)) becomes exponentially suppressed in this case[3]. For example, at a density $n = 10^{10}\,\mathrm{cm}^{-3}$, the fractional atom loss rate $\dot{n}/n = 0.06\,\mathrm{s}^{-1}$ is significantly reduced but the critical temperature $T_c \sim 10^{-7} T_F$ has been exponentially suppressed.

By confining atoms in an optical lattice potential, the BCS critical temperature can be exponentially increased even though the gas remains at low density. This is done by quenching the kinetic energy of the atoms (i.e. giving them a large effective mass) so that attractive interactions become strong in comparison [22]. To create a 3D cubic optical lattice, six laser beams are configured such that pairs of beams counterpropagate along each of three orthogonal axes. This generates a potential of the form $V(\mathbf{r}) = V_0(\cos^2(k_L x) + \cos^2(k_L y) + \cos^2(k_L z))$, where k_L is the laser wavenumber and V_0 is the depth typically measured in units of the photon recoil energy ($E_R = \hbar^2 k_L^2/2m$). For atoms confined in the lowest Bloch band of this periodic potential, the system can be described by the Hubbard Hamiltonian equation (4). For an optical lattice of depth $V_0 = s\,E_R$, the tunneling matrix element $t = E_R(2/\sqrt{\pi})s^{3/2}\exp(-2\sqrt{s})$ and on-site interaction energy $U = E_R a_t k_L \sqrt{8/\pi}\, s^{3/2}$ in the tight-binding limit. Note that t, which determines the width of the lowest band ($12t$ for a 3D cubic lattice) and is inversely proportional to the effective mass, is exponentially reduced as the depth V_0 is increased.

Quite generically, the BCS critical temperature in the weak coupling limit can be estimated as $T_c \sim E_F \exp[-1/(\mathcal{D}(E_F)\,U)]$, where $\mathcal{D}(E_F)$ is the density of states at the Fermi surface and U is the interaction strength. For a fixed interaction strength, the critical temperature can be exponentially increased by increasing the density of states at the Fermi surface. For a homogeneous system in the absence of an optical lattice, the critical temperature is exponentially increased by increasing the density of the gas and thereby increasing E_F and $\mathcal{D}(E_F)$ (since $\mathcal{D}(E) \propto \sqrt{E}$). In the case of an optical lattice, on the other hand, the density of states is increased by exponentially reducing the width of the lowest band with increasing lattice depth so that the density of states at the Fermi energy $\mathcal{D}(E_F)$ is made large even though E_F remains small. For a 3D cubic lattice at half-filling, for example, the Fermi energy $E_F = 6t$ and $\mathcal{D}(E_F) = 1/7t$ (where t is the tunneling matrix element) and the critical temperature $T_c \sim 6t\exp[-7t/|U|]$, where U is the on-site interaction energy. The tunneling matrix element is exponentially reduced as the depth of the lattice is increased, allowing for a dramatic increase in T_c with only a modest increase in density.

When $\mathcal{D}(E_F)\,U$ becomes of the order of unity or larger, the weak coupling BCS picture breaks down and cannot be used to predict T_c. In order to provide an estimate of experimental lattice and gas parameters that maximize T_c, we provide here a heuristic argument. We will consider a three-component Fermi gas confined in a 3D cubic lattice at one-third filling and make the crude approximation that pairing is so strong that the gas becomes completely magnetized (see figure 2(a)) forming domains that each contain only two species. In each of these domains, the lattice is now at half-filling for the two species. The critical temperature for a two-component Fermi gas in a 3D cubic lattice at half-filling can be found exactly from quantum Monte Carlo calculations [23]. Figure 2(b) shows the critical temperature in units of t as a function of $|U|/t$. The black dots are a quantum Monte Carlo calculation of the Neél temperature for the repulsive Hubbard model at half-filling [23], which, through the repulsive–attractive transformation of the Hubbard model at half-filling, is identical to T_c. The

[3] We consider the BCS critical temperature here (rather than that for the strong-coupling limit) since the strong coupling limit requires $n \gtrsim 3 \times 10^{12}$ atoms cm^{-3} in order for $k_F\,a_t \gtrsim 1$, and the BCS critical temperature is therefore the relevant one as the density is reduced below this value.

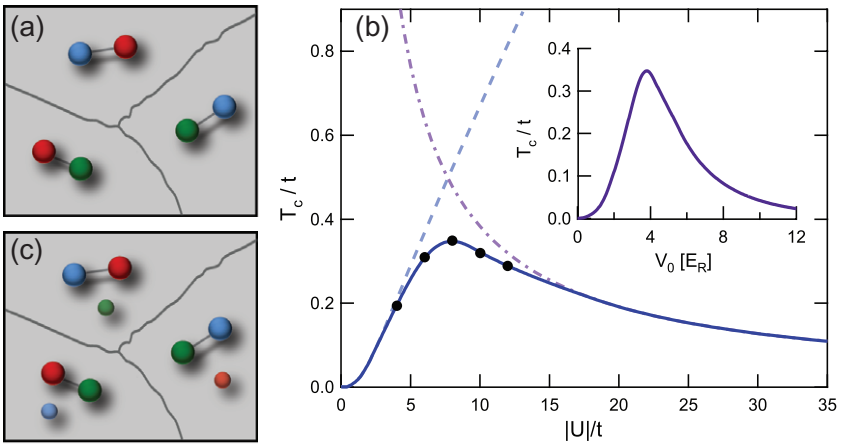

Figure 2. Cooper pairing and magnetization in an optical lattice at 1/3-filling. In an SU(3)-symmetric system of three particles with attractive interactions, Cooper pairing is equally likely between any antisymmetric combination of distinguishable fermions. (a) If the attractive interactions are sufficiently strong, the particles phase separate into domains each containing two distinguishable particles so that all particles can participate in Cooper pairing. For such a complete phase separation, the increase in local Fermi energy ($\sim t$) must be offset by the decrease in energy due to Cooper pairing. (b) To estimate the pair binding energy, we consider a domain that contains only two distinguishable states. In this case, the superfluid critical temperature in an optical lattice can be calculated using the repulsive–attractive transformation of the Hubbard model (see text). (c) The reduction in energy due to Cooper pairing ($\lesssim 0.6\,t$) will not be sufficient to overcome the increase in local Fermi energy ($\approx t$) required for complete phase separation and only partial polarization will be achieved. Thus, domains will form in which the numbers of particles of one color will be fewer than those of the other two, but will not be zero.

quantum Monte Carlo calculations are joined by a smoothing spline (solid blue) to Hartree–Fock theory (dashed light blue) in the weak coupling limit and a solution of the spin-1/2 Heisenberg model (dot-dashed purple) in the strong coupling limit [23]. The inset shows the same T_c now plotted as a function of V_0 in units of E_R assuming that $a = -2222\,a_0$ and a lattice constant of $d = 3.22\,\mu$m. Thus, for a two-component Fermi gas at half-filling, T_c can be as high as $T_c \simeq 0.35\,t$. This maximum in T_c corresponds to a lattice depth $V_0 = 3.8\,E_R$ for the given parameters. Note that the average density of atoms in each internal state is $n_\alpha \simeq 10^{10}\,\mathrm{cm}^{-3}$ for a lattice at one-third filling. While this argument relied on our assumption of complete magnetization, which may not be entirely fulfilled, we will use these parameters moving forward as we assess the feasibility of achieving color superfluidity in this system.

For a 3D cubic lattice at one-third filling, the Fermi energy $E_F = 4.8\,t$ and the superfluid critical temperature may be as high as $T_c \simeq 0.07\,T_F$. To reach the superfluid transition, a reduced temperature $T/T_F < 0.07$ must be achieved in free space prior to loading atoms into the optical lattice since T/T_F remains approximately constant as the lattice potential is increasing adiabatically [24]. Given the large three-body recombination rate in three-component Fermi gases, we will now assess whether such temperatures can be achieved.

As stated previously, the state-of-the-art for cooling two-component Fermi gases is $T = 0.05 T_F$. We now show that a degenerate three-component Fermi gas can be created from a two-component Fermi gas at a reduced temperature $T/T_F = 0.05$ with no additional evaporative cooling. A RF magnetic field can be used to populate all three internal states starting from a two-component Fermi gas by driving transitions between states $|1\rangle$–$|2\rangle$ and $|2\rangle$–$|3\rangle$ [19]. If these RF transitions are driven in the presence of a magnetic field gradient, an incoherent three-component mixture with equal populations in each state is created. In the absence of collisions, the three-component Fermi gas so produced would not be in a thermal state. However, since the three distinguishable fermions will collide, the mixture will equilibrate at a new reduced temperature $\tau' = T'/T_F'$. Since the RF field neither adds nor removes kinetic energy from the system, we can determine τ' by equating the total energy in the two-component gas at initial reduced temperature $\tau = T/T_F$ with the total energy in the three-component gas at reduced temperature τ',

$$2\int_0^\infty \epsilon\, f(\epsilon,\tau)\,\mathcal{D}(\epsilon)\,\mathrm{d}\epsilon = 3\int_0^\infty \epsilon\, f(\epsilon,\tau')\,\mathcal{D}(\epsilon)\,\mathrm{d}\epsilon. \tag{5}$$

Here, $f(\epsilon,\tau) = [\exp[(\epsilon - \mu/E_F)/\tau] + 1]^{-1}$ is the Fermi–Dirac distribution function, ϵ is the energy in units of E_F and $\mathcal{D}(\epsilon)$ is the density of states. For a homogeneous system, this condition reduces to $2^{2/3}(\tau')^{5/2}\mathrm{Li}_{5/2}(-\mathcal{Z}(\tau')) = 3^{2/3}\tau^{5/2}\mathrm{Li}_{5/2}(-\mathcal{Z}(\tau))$, where Li_n is the polylogarithm function and $\mathcal{Z}(\tau) = \exp[\mu/(E_F\tau)]$ is the fugacity. For a given initial reduced temperature, numerical root finding gives the reduced temperature τ' of the three-component gas after equilibration. For example, for $\tau = 0.1$, we find that $\tau' = 0.33$, and for $\tau = 0.05$, we find that $\tau' = 0.31$. Thus, a degenerate three-component Fermi gas can be produced from a degenerate two-component Fermi gas without any further evaporative cooling. However, achieving the higher degree of degeneracy required to observe color superfluidity will require a modest amount of evaporative cooling.

Successful evaporative cooling requires that the ratio of the elastic collision rate to the trap loss rate is made as large as possible. As a point of reference, the necessary condition for runaway evaporative cooling of a thermal gas in a linear trapping potential is that the ratio between good and bad collision rates is $\gtrsim 100$ [25]. Here we compare the elastic collision rate in a three-component Fermi gas with the loss rate due to three-body recombination. The elastic collision rate obtained from the quantum Boltzmann equation (assuming ergodicity) is [26]

$$\Gamma = \frac{m\sigma}{N\pi^2\hbar^3}\int \mathrm{d}\epsilon_1\,\mathrm{d}\epsilon_2\,\mathrm{d}\epsilon_3\,\mathrm{d}\epsilon_4\,\delta(\epsilon_1+\epsilon_2-\epsilon_3-\epsilon_4)\,\mathcal{D}(\epsilon_{\min})\,f(\epsilon_1)\,f(\epsilon_2)\,[1-f(\epsilon_3)]\,[1-f(\epsilon_4)].$$

Here, $\epsilon_{\min} = \min(\epsilon_1,\epsilon_2,\epsilon_3,\epsilon_4)$ and $\sigma = 8\pi a^2$. This equation describes particles in states with energy ϵ_1 and ϵ_2 scattering into states with energy ϵ_3 and ϵ_4. Note that the elastic collision rate is reduced by Pauli blocking due to the $[1 - f(\epsilon)]$ terms, which inhibit scattering into the final states if the occupation in those states approaches unity. The collision rate Γ (obtained from numerical integration) for a three-component Fermi gas at temperature $T = 0.3\,T_F$, density $n_\alpha = 10^{10}\,\mathrm{cm}^{-3}$ (in each spin state) and $a = -2222\,a_0$ is $\Gamma \simeq 8\,\mathrm{s}^{-1}$. The corresponding three-body recombination rate $\dot{n}_\alpha/n_\alpha = -K_3 n^2 = -0.06\,\mathrm{s}^{-1}$. Thus, the ratio between good and bad collisions is $\simeq 140$. Conditions are therefore favorable for further evaporative cooling to reduce the temperature of an already degenerate Fermi gas to $T < 0.07\,T_F$.

Assuming that a three-component Fermi gas with $T < 0.07\,T_F$ is prepared by evaporative cooling, color superfluidity can be achieved by adiabatically increasing the depth of the optical

lattice to a value $V_0 \simeq 4E_R$. If the lattice is increased adiabatically (i.e. at fixed entropy), the ratio T/T_F remains approximately constant in a homogeneous system [24]. Determining the time scale required for adiabaticity in an interacting many-body system is beyond the scope of this paper. However, we can make several general remarks. When the lattice is applied, the dispersion relation, in the tight binding limit, becomes $E(\mathbf{k}) = -2t[\cos(k_x d) + \cos(k_y d) + \cos(k_z d)]$ and hence is anisotropic. Thus, the application of the lattice requires a change in the shape of the Fermi surface and a redistribution of occupation numbers in k-space. The change in the Fermi surface is most dramatic when the lattice depth increases from zero to $V_0 \simeq 1E_R$ [22]. The timescale required to increase the depth to $V_0 = 1E_R$ must therefore be long compared with the collision time in order to allow for a redistribution in k-space. Alternatively, the lattice can be increased to $V_0 = 1E_R$ simultaneously with the final stage of evaporative cooling. This does not produce significantly more loss due to three-body recombination during evaporation since the increase in density is very modest. As the lattice is turned on, the density at the center of each site will be increased above the mean density averaged over many sites, n_0. For the spatially dependent density that results, the three-body recombination loss rate $\dot{N}/N = -K_3 \langle n^2 \rangle$, where $\langle n^2 \rangle$ is the squared density averaged over a unit cell of the lattice. At a depth of $V_0 = 1E_R$, the averaged square density $\langle n^2 \rangle \simeq 1.3n_0^2$, resulting in a 30% higher loss rate during evaporation. Once a Fermi gas at $T/T_F < 0.07$ is prepared in a $V_0 = 1E_R$ deep lattice by evaporative cooling, the lattice depth can be increased relatively rapidly to $V_0 \simeq 4E_R$ since the change in shape of the Fermi surface is much less dramatic. To maintain constant entropy, the occupation number in k-space does not need to change significantly. Changing the depth of the lattice too rapidly does not change the quasi-momentum $\mathbf{k}$ but can cause interband excitation. So the depth of the lattice should be raised on a timescale that is long compared with h/E_R since the band gap $\sim E_R$. For ^{6}Li atoms in a lattice with $d = 3.22\,\mu$m, the lattice can be raised over a time of $10 \times h/E_R \simeq 13$ ms. Once the depth of the lattice is $V_0 = 4E_R$, the three-body recombination rate will be increased due to the increase in density. For $V_0 = 4E_R$, the averaged square density $\langle n^2 \rangle \simeq 10\,n_0^2$, and the three-body loss rate is ten times higher than that obtained in the absence of the lattice (i.e. $\dot{N}/N = -K_3 \langle n^2 \rangle = -0.6\,\mathrm{s}^{-1}$ for the parameters suggested above for the ^{6}Li system). This loss rate should be sufficiently low to allow for Cooper pair formation, which occurs on a timescale $\sim h/\Delta_0 \simeq 2\,h/t$ (e.g. $2\,h/t \simeq 40$ ms for the ^{6}Li system).

The approach outlined above minimizes the detrimental effects of three-body loss by working with low-density atomic samples confined in a large-period optical lattice. In this case, the rate at which occupation on a triply occupied lattice site decays due to three-body recombination, γ_3, is much smaller than $t/\hbar$ (i.e. the tunneling rate). Alternatively, the authors of [27] have recently proposed that loss due to three-body recombination can also be suppressed by working in the opposite limit where $\gamma_3 \gg t/\hbar$. Here, rapid three-body recombination provides a mechanism for continuously measuring the number of lattice sites that have triple occupancy and, by the quantum Zeno effect, constrains the evolution of the system such that lattice sites never become triply occupied. In addition to suppressing loss due to three-body recombination, the constraint that triply occupied sites are absent stabilizes the color superfluid phase against the formation of a trionic phase at strong coupling. Suppression of the trionic phase has now been predicted for 1D [27] and higher-dimensional [28] systems. Thus, the constrained case (corresponding to $\gamma_3 \gg t/\hbar$) is of interest for the study of the color superfluid phase in the weak, intermediate and strong coupling limits, whereas the unconstrained case

(corresponding to $\gamma_3 \ll t/\hbar$ as considered in this paper) may allow for observing the phase transition between a color superfluid and a Fermi liquid of trimers.

5. Realizing SU(3)-invariant interactions

Our discussion of superfluidity in a three-component Fermi gas has so far assumed that the three pairwise scattering lengths are identical and that the Hamiltonian in equation (1) is SU(3) symmetric. In reality, the three scattering lengths for a three-component alkali gas will be nearly, but not exactly, equal for a large but finite bias field.[4] In the case of ^{6}Li, the interaction between states $|1\rangle$ and $|2\rangle$ is the most attractive (i.e. $a_{12} < a_{23} < a_{13}$). This anisotropy can fundamentally alter the character of the superfluid phase. For example, the anisotropy of the interactions breaks the SU(3) symmetry and can lock the three-component superfluid order parameter so that only $\Delta_{12} \neq 0$. In this case, the color superfluid phase is an essentially standard U(1) superfluid in the presence of a decoupled Fermi liquid of atoms in state $|3\rangle$ [14]. Since only the U(1) symmetry is spontaneously broken in this case, a single NG mode exists rather than five. Perhaps most dramatically, breaking the SU(3) has existential implications for vortices. In a system with perfect SU(3) symmetry, Rapp *et al* [14] point out that any vortex can be twisted away due to the large internal symmetry of the order parameter, whereas vortices can exist in a U(1) superfluid. Finally, anisotropic interactions may change the nature of the phase transition between superfluidity and a Fermi gas of trimers from a second-order phase transition to one of first order [14]. For these reasons, it is worthwhile exploring methods to reduce the difference between scattering lengths to arbitrarily small levels. In this section, we describe how changes in scattering lengths can be affected by applying RF radiation to reduce the difference between scattering lengths in the ^{6}Li system by more than one order of magnitude. In this case, the difference between on-site interaction energies U for different pairs is at least one order of magnitude smaller than any other energy scale in the system, including the pairing gap. Further, we suggest that the application of an MW field in addition to the RF field can allow for independent tuning of the three scattering lengths and the realization of perfect SU(3) symmetry.

When RF radiation is near resonant with a transition between two atomic Zeeman states (see figure 3(a)), the eigenstates of the composite atom+field system (i.e. the RF-dressed states) contain an admixture of the two coupled Zeeman states. When two such RF-dressed atoms collide, the scattering properties in the dressed channel sample the scattering properties of all of the undressed two-body collision channels that have now been coupled by the RF field [29, 30]. Thus, if the scattering lengths in two or more undressed collision channels differ substantially, controlled RF coupling of these channels can be used to tune the scattering lengths in the dressed channels. Using a simple model, we calculate below how the scattering lengths in a three-component ^{6}Li mixture can be tuned by applying RF fields to achieve nearly perfect SU(3) symmetry. The use of RF or MW radiation to control scattering lengths in other atoms or in other contexts has also been considered recently in [29–33].

Before computing scattering matrix elements for dressed state collisions, we first identify an appropriate basis to describe the asymptotically separated two-body wavefunction (i.e. the scattering channels). In the presence of RF radiation, the RF photon field and the internal states

[4] For the three-component ^{6}Li gas under consideration, the three scattering lengths are within 2% of the average value at a field of 2000 G.

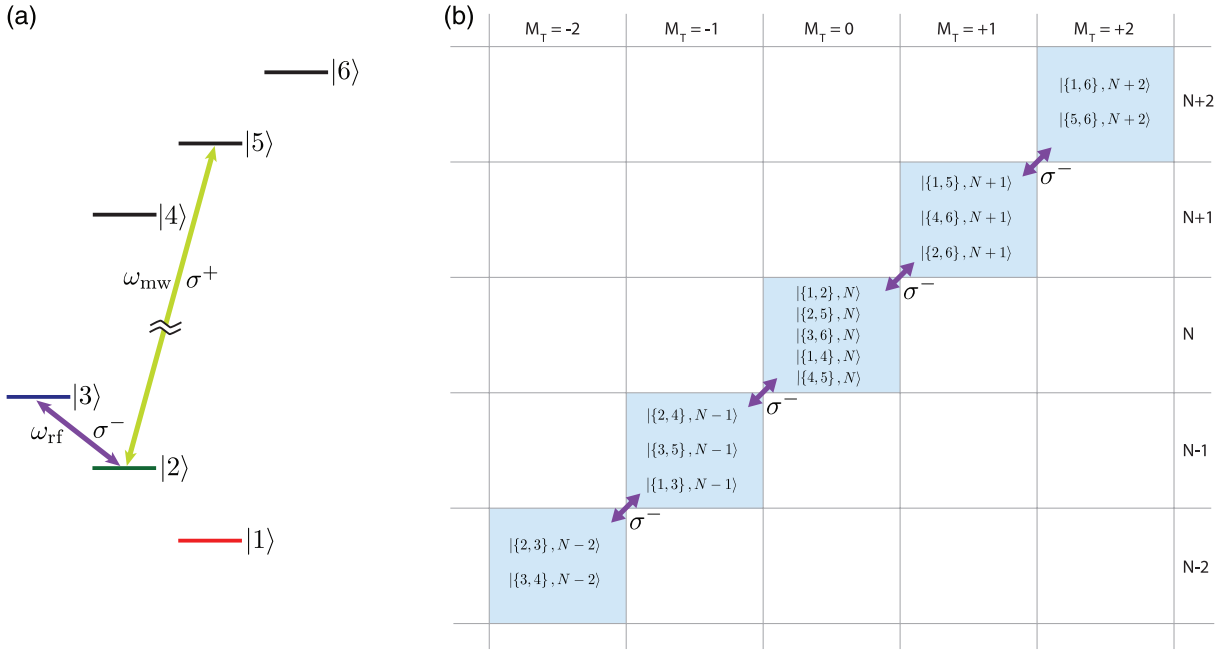

Figure 3. (a) An RF (MW) magnetic field near resonance with the $|2\rangle$–$|3\rangle$ ($|2\rangle$–$|5\rangle$) transition creates photon-dressed states that sample the collision properties of the collision channels, which are coupled. (b) The 15 bare collision channel states that are coupled by the σ^--polarized RF field in (a). The notation $|\{\alpha, \beta\}, N_0\rangle$ denotes the product of an antisymmetric combination of Zeeman states $|\alpha\rangle$ and $|\beta\rangle$ and a photon number state $|N_0\rangle$.

of asymptotically separated atoms are eigenstates of $H_A + H_\gamma + H_{A\gamma}$, where

$$H_A = \frac{A_{hf}}{\hbar^2}\sum_{k=1,2}\mathbf{I}_k\cdot\mathbf{S}_k - \frac{\mu_B B_0}{\hbar}\sum_{k=1,2}\left(g_s\mathbf{S}_k\cdot\hat{\mathbf{z}} + g_i\mathbf{I}_k\cdot\hat{\mathbf{z}}\right), \qquad H_\gamma = \hbar\omega_{rf}a^\dagger a$$
$$H_{A\gamma} = -\eta_s\sum_{k=1,2}\left[\left(\hat{\mathbf{e}}\cdot\mathbf{S}_k\right)a + \left(\hat{\mathbf{e}}^*\cdot\mathbf{S}_k\right)a^\dagger\right] - \eta_i\sum_{k=1,2}\left[\left(\hat{\mathbf{e}}\cdot\mathbf{I}_k\right)a + \left(\hat{\mathbf{e}}^*\cdot\mathbf{I}_k\right)a^\dagger\right] \tag{6}$$

are the atomic internal state Hamiltonian, the Hamiltonian for the RF field and the atom–photon coupling Hamiltonian, respectively. Here, A_{hf} is the hyperfine constant, $\mathbf{S}_k$ and $\mathbf{I}_k$ are, respectively, the electron and nuclear spins for each atom, μ_B is the Bohr magneton, B_0 is the bias magnetic field in the $\hat{\mathbf{z}}$ direction, g_s and g_i are the g-factors for the electron and nuclear spin, ω_{rf} is the frequency of the RF photon, $a^\dagger$ (a) is the creation (annihilation) operator for a RF photon, $\hat{\mathbf{e}}$ is the polarization vector of the RF magnetic field and $\eta_{s/i}$ are the coupling constants between the electron/nuclear spin and the photon field. For a field mode of frequency ω_{rf} in a volume V, the coupling constants $\eta_{s/i} = g_{s/i}\,\mu_B\sqrt{\frac{\hbar\omega_{rf}}{2\epsilon_0 c^2 V}}$. Eigenstates of $H_A + H_\gamma + H_{A\gamma}$, which are antisymmetric under exchange of the fermionic particle labels, are used as basis states to calculate the scattering matrix elements for s-wave collisions at threshold. These are identical to the basis states used in [30].

In this paper, we will limit our attention to a circularly polarized RF magnetic field since the number of channel states in this case is finite and inelastic collision rates are minimized [30]. In the absence of RF–atom coupling (i.e. for $H_{A\gamma} = 0$), the bare basis states $|\{a, b\}, N\rangle$, which are

the product of a photon number state ($|N\rangle$) and an antisymmetric combination of Zeeman states ($|\{a,b\}\rangle = \frac{1}{\sqrt{2}}(|a\rangle|b\rangle - |b\rangle|a\rangle)$), are eigenstates of $H_{\rm A} + H_\gamma$. These states become coupled when $H_{{\rm A}\gamma}$ is nonzero. For a circularly polarized RF field, $H_{{\rm A}\gamma}$ couples the subset of bare basis states that have the same projection of the total angular momentum (for atom plus photons) along the $\hat{\mathbf{z}}$ axis. The 15 bare basis states coupled in the case of σ^- polarized RF radiation are shown in figure 3(b). The eigenstates of equation (7) (which, in practice, are found in terms of the bare basis states) are the dressed channel states that we use as the basis to represent the scattering matrix. When we diagonalize equation (7), we assume that $a^\dagger|N\rangle \simeq \sqrt{\langle N\rangle}|N+1\rangle$ (and $a|N\rangle \simeq \sqrt{\langle N\rangle}|N-1\rangle$) since the average number of photons in the RF field, $\langle N\rangle$, is very large. Further, we assume that the classical amplitude of the RF magnetic field is given by $B_{\rm rf} = 2\sqrt{\frac{\hbar\omega_{\rm rf}}{2\epsilon_0 c^2 V}}\sqrt{\langle N\rangle}$, as would be the case if the RF field were a coherent state with $\langle a^\dagger a\rangle = \langle N\rangle$.

Having found the RF-dressed channel states, we find the scattering matrix elements by solving a coupled channel Schrödinger equation for s-wave scattering, using as our Hamiltonian

$$H_{\rm scatt} = \frac{\mathbf{p}^2}{2\mu} + V_{\rm S}(r)\mathcal{P}^{(\rm S)} + V_{\rm T}(r)\mathcal{P}^{(\rm T)} + H_{\rm A} + H_\gamma + H_{{\rm A}\gamma}, \tag{7}$$

where $\mathbf{r}$ is the relative separation of the atoms, $\mathbf{p}$ is the relative momentum and μ is the reduced mass. The molecular interaction between two alkali atoms is given by $V(r) = V_{\rm S}(r)\mathcal{P}^{(\rm S)} + V_{\rm T}(r)\mathcal{P}^{(\rm T)}$, where $V_{\rm S}(r)$ ($V_{\rm T}(r)$) is the singlet (triplet) molecular potential and $\mathcal{P}^{(\rm S)}$ ($\mathcal{P}^{(\rm T)}$) denotes a projection operator onto the subspace of singlet (triplet) states of the valence electrons.[5] To dramatically simplify the solution of the full coupled channel problem, we make two approximations. First, we use square-well potentials to represent the singlet and triplet molecular potentials. The square-well potentials have the same radius R but different depths, $V_{0,\rm S}$ and $V_{0,\rm T}$. The parameters R, $V_{0,\rm S}$ and $V_{0,\rm T}$ are chosen to reproduce the known singlet and triplet scattering lengths, $a_{\rm s}$ and $a_{\rm t}$, and the binding energy, $E_{\rm b}$, of the highest-lying bound state of the singlet molecular potential for $^6{\rm Li}_2$ dimers. Our second assumption is that $H_{\rm scatt}$ is diagonal in the singlet–triplet basis for $r < R$, where the singlet and triplet molecular potentials dominate over the hyperfine interaction and the RF coupling. This simple model reproduces, to a good approximation, all of the scattering properties for ^{6}Li s-wave collisions reported in the literature. For example, the location and widths of the three Feshbach resonances shown in figure 1, which all result from the presence of the highest-lying bound state in the singlet molecular potential, are reproduced by this simple model.

To find the threshold scattering properties for a given RF-dressed entrance channel $|\alpha\rangle$, we solve the coupled channel Schrödinger equation to first order in the relative wavenumber k of the colliding atoms. The solution of the coupled channel Schrödinger equation gives the scattering matrix elements $S_{\beta,\beta'}$ between dressed channel states $|\beta\rangle$ and $|\beta'\rangle$. We extract the s-wave scattering length a_α for the entrance channel $|\alpha\rangle$ from the diagonal S-matrix element $S_{\alpha,\alpha}$ using the relation $S_{\alpha,\alpha} = \exp(-2ik\tilde{a}_\alpha) \simeq 1 - 2ik\,\tilde{a}_\alpha$, where $\tilde{a}_\alpha = a_\alpha - ib_\alpha$ is the complex scattering length. If $b_\alpha > 0$, there are other open channel states into which $|\alpha\rangle$ can scatter. The threshold rate constant for scattering into these open channels is given by

$$K_2 = \lim_{k\to 0}\frac{\pi\hbar}{\mu k}\sum_{\beta\neq\alpha}\left|S_{\alpha,\beta}(k)\right|^2.$$

The relationship between b_α and K_2 is given by $K_2 = \frac{2h}{\mu}b_\alpha$.

[5] We ignore weak relativistic spin-dependent interactions in this calculation.

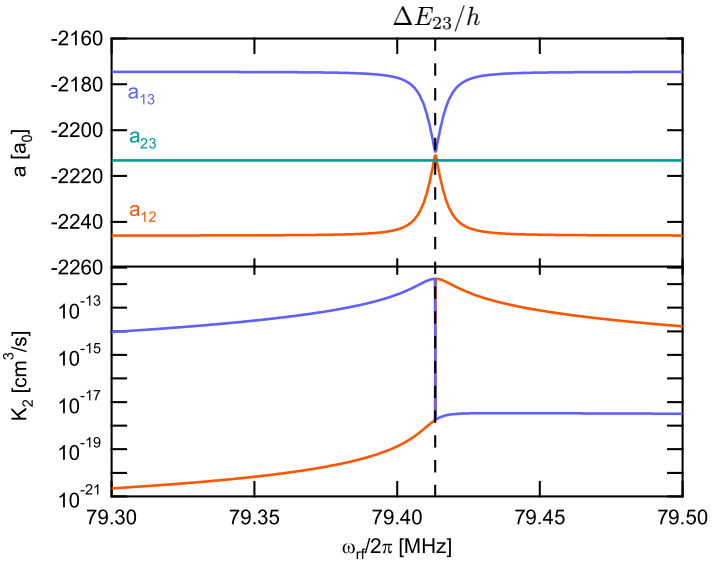

Figure 4. (Upper panel) The scattering lengths a_{12}, a_{23} and a_{13} in a $B_0 = 2000\,\mathrm{G}$ bias field as a function of RF frequency ω_{rf} for an RF field amplitude $B_{\mathrm{rf}} = 140\,\mathrm{mG}$. When ω_{rf} is resonant with the $|2\rangle$–$|3\rangle$ transition, all three scattering lengths are equal to 1 part in 1000. (Lower panel) The associated two-body inelastic rate constants K_2. Since we neglect spin–spin dipole interactions, the inelastic loss rate constant associated with a_{23} is identically zero.

RF-dressing of scattering states can be used to significantly reduce the difference in pairwise scattering lengths in a three-component Fermi gas. As a demonstration, we calculate the scattering lengths and inelastic decay rate constants for RF-dressed collision channels of ^{6}Li atoms in a $B_0 = 2000\,\mathrm{G}$ bias field with a σ^--polarized RF magnetic field tuned near the $|2\rangle$–$|3\rangle$ transition (see figure 3(a)). The amplitude of the RF field is $B_{\mathrm{rf}} = 140\,\mathrm{mG}$. The RF field strongly couples the bare collision channels $|\{1, 2\}, N\rangle$ and $|\{1, 3\}, N-1\rangle$. The scattering lengths $(a_{12}(\omega_{\mathrm{rf}}),\ a_{13}(\omega_{\mathrm{rf}}))$ and inelastic decay rate constants for the RF-dressed collision channels associated with these bare channels are shown in figure 4. Also shown is the scattering length $a_{23}(\omega_{\mathrm{rf}})$ associated with the bare scattering channel $|\{2, 3\}, N-2\rangle$, which is not coupled to other bare scattering channels. For the $|\{2, 3\}, N-2\rangle$ channel, the inelastic decay rate constant is identically zero for our model since we neglect weak spin–spin dipole interactions.

At a field of 2000 G and for a RF field resonant with the $|2\rangle$–$|3\rangle$ transition (at $\omega_{\mathrm{rf}}/2\pi = 79.413\,\mathrm{MHz}$), the three scattering lengths $a_{12}(\omega_{\mathrm{rf}})$, $a_{23}(\omega_{\mathrm{rf}})$ and $a_{13}(\omega_{\mathrm{rf}})$ are approximately equal (to better than 1 part in 1000), as shown in figure 4(a). On resonance, the scattering lengths $a_{12}(\omega_{\mathrm{rf}})$ and $a_{13}(\omega_{\mathrm{rf}})$ are equal and approximately given by the average value of the scattering lengths a_{12} and a_{13} in the absence of RF coupling. Because $a_{23} \simeq (a_{13} + a_{23})/2$ in the absence of RF coupling, all three scattering lengths are made nearly equal for resonant RF. Exactly on resonance, the three scattering lengths differ from their average by less than 1 part in 1000. Thus, RF dressing of the collision channels achieves in this case a reduction in the difference between scattering lengths by more than one order of magnitude. The two-body inelastic rate

constant for the RF-dressed channel states associated with $|\{1,2\},N\rangle$ and $|\{1,3\},N-1\rangle$ are both $K_2 = 1.64\times10^{-12}\,\mathrm{cm^3\,s^{-1}}$ on resonance. For a low-density gas such as that discussed in section 4, this two-body decay rate constant is sufficiently small that it will not cause significant loss of atoms over the timescale required for equilibration. This example shows that by using RF radiation resonant with the $|2\rangle$–$|3\rangle$ transition, we can reduce the difference between scattering lengths for a three-component Fermi gas to the point where the associated difference between on-site interaction energies is an order of magnitude smaller than the pairing gap Δ_0.

We have also considered whether further reductions in the difference between scattering lengths can be achieved by applying an MW radiation field. In the case just considered, we achieved nearly identical scattering lengths by resonantly coupling the bare $|\{1,2\},N\rangle$ and $|\{1,3\},N-1\rangle$ collision channels with RF radiation and found that, on resonance, $a_{12}(\omega_{\rm rf}) = a_{13}(\omega_{\rm rf}) = (a_{12}+a_{23})/2$, which is close to the value of a_{23}. If it were the case that $a_{23} = (a_{12}+a_{23})/2$, all three RF-dressed scattering lengths could be made identical by this technique. We now consider whether we can tune a_{12} and a_{23} by applying a MW radiation field so that $a_{23} = (a_{12}+a_{23})/2$. We expect that, in this case, the application of both the RF- and MW-dressing fields will allow the realization of a system with identical scattering lengths.

To tune the a_{12} and a_{23} scattering lengths, we consider applying a σ^+-polarized MW magnetic field nearly resonant with the $|2\rangle$–$|5\rangle$ transition, as shown in figure 3(a). This MW field couples together the bare $|\{1,2\},N\rangle$ and $|\{1,5\},N+1\rangle$ collision channels and it also couples the bare $|\{2,3\},N-2\rangle$ and $|\{3,5\},N-1\rangle$ collision channels. The scattering lengths for the MW-dressed channels are shown in figure 5 along with the two-body decay rate constants. For these calculations, the bias field $B_0 = 2000\,\mathrm{G}$ and the amplitude of the MW magnetic field is $B_{\rm mw} = 140\,\mathrm{mG}$. Figure 5(a) shows that the scattering lengths $a_{12}(\omega_{\rm mw})$ and $a_{15}(\omega_{\rm mw})$ can change significantly near resonance due to the fact that the scattering lengths of the two bare channels (i.e. the scattering lengths away from resonance) are substantially different. Similarly, as shown in figure 5(b), the scattering lengths $a_{23}(\omega_{\rm mw})$ and $a_{35}(\omega_{\rm mw})$ change significantly near resonance. Near resonance, the two-body inelastic decay rate constants can be very large. An exceptional case, however, is the dressed channel associated with the $|\{1,2\},N\rangle$ state. In this case, $a_{12}(\omega_{\rm mw})$ can be changed substantially for MW frequencies tuned below the resonance condition and K_2 remains extremely small. Thus, MW-dressing may be useful in controlling the interactions in two-component Fermi gases that have population in states $|1\rangle$ and $|2\rangle$.

In the present context, that of making slight changes in the a_{12} and a_{23} scattering lengths, we find that small changes can be made using MW radiation far from resonance where K_2 is reduced from its maximum value. For example, in figure 6, we plot the scattering lengths $a_{12}(\omega_{\rm mw})$, $a_{23}(\omega_{\rm mw})$ and $a_{13}(\omega_{\rm mw})$, along with the associated two-body decay rate constants, for MW frequencies below the $|2\rangle$–$|5\rangle$ resonance. For a MW frequency of 5.958 GHz, the average of $a_{12}(\omega_{\rm mw})$ and $a_{13}(\omega\mathrm{mw})$ is exactly equal to $a_{23}(\omega_{\rm mw})$. It is for this MW power and frequency that we expect that the application of a separate RF field resonant with the $|2\rangle$–$|3\rangle$ transition will create a three-component mixture with identically equal scattering lengths. In this case, the largest two-body decay rate constant $K_2 = 2\times10^{-11}\,\mathrm{cm^3\,s^{-1}}$ occurs in the MW-dressed channel associated with $|\{2,3\},N-2\rangle$. This two-body decay rate constant is sufficiently small that for a ^{6}Li Fermi gas with $n_\alpha = 10^{-10}\,\mathrm{cm^{-3}}$, as considered in section 4, the equilibration time is much shorter than the timescale for atom loss. These calculations indicate that it is possible to make a three-component ^{6}Li Fermi gas with an exact SU(3) symmetry.

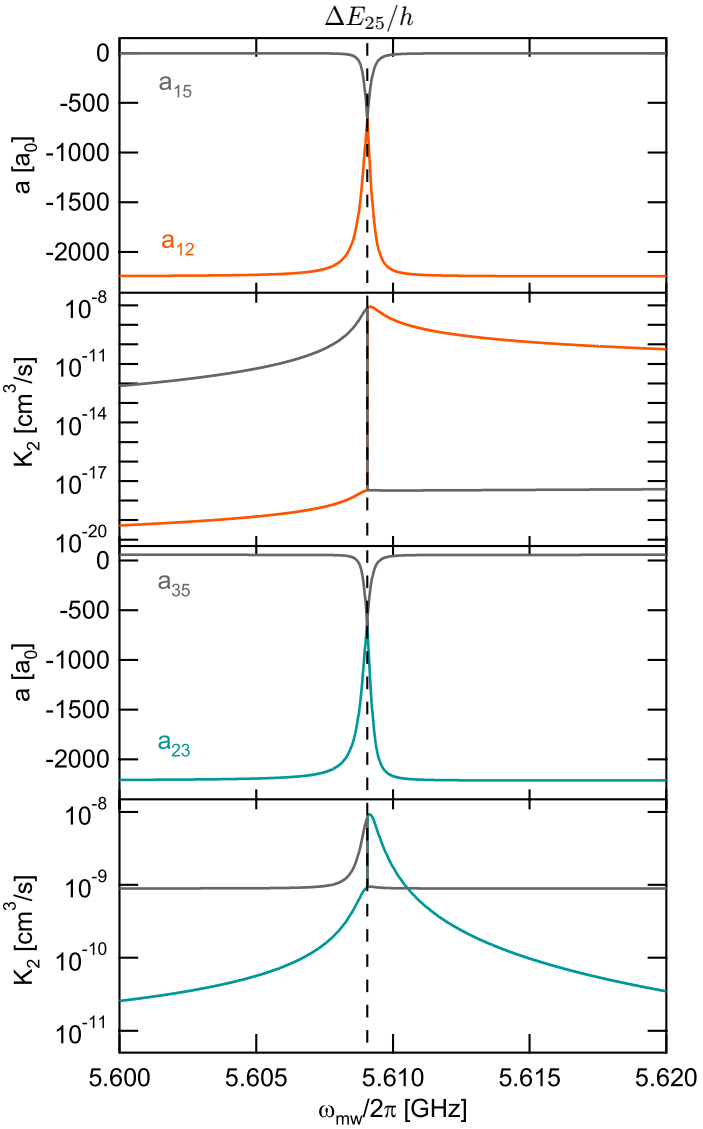

Figure 5. (a) The a_{12} and a_{15} scattering lengths in a bias magnetic field $B_0 = 2000\,\mathrm{G}$ as a function of MW frequency ω_{mw} for a σ^+-polarized MW field with an amplitude $B_{\mathrm{mw}} = 140\,\mathrm{mG}$. (b) The two-body inelastic rate constants K_2 associated with a_{12} and a_{15}. (c) The a_{23} and a_{35} scattering lengths for the same parameters as in (a). (d) The two-body inelastic rate constants K_2 associated with a_{23} and a_{35}.

6. Analogues of color superconductivity with color and spin

A marked difference between quark matter and the three-component Fermi gas described so far is that quark matter has spin and flavor degrees of freedom in addition to color. The numerous degrees of freedom available in quark matter make many different patterns of Cooper pairing possible. Deciding which of these pairing patterns are favored by nature, particularly in the presence of strong interactions and imbalanced Fermi surfaces, is a significant challenge in the

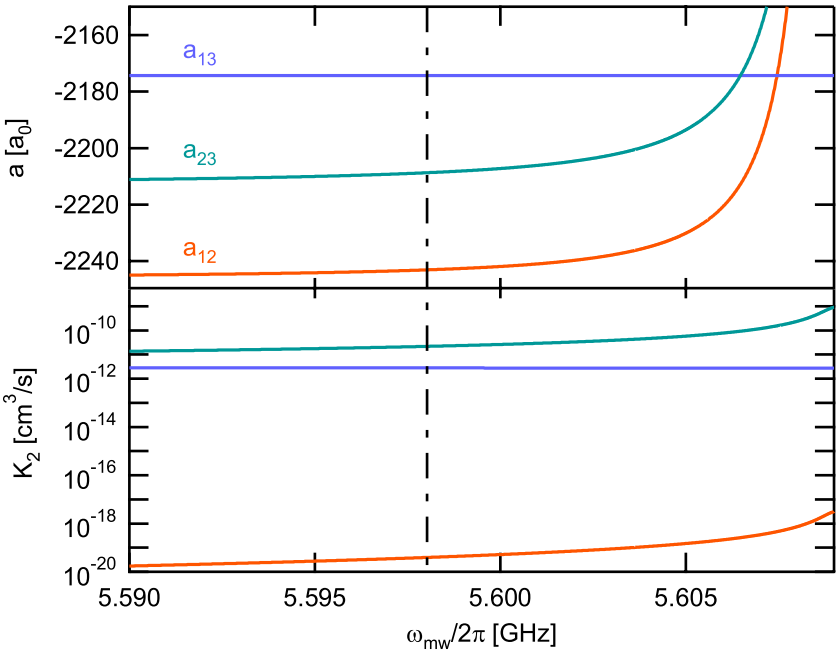

Figure 6. (Upper panel) The a_{12}, a_{23} and a_{13} scattering lengths in a bias magnetic field $B_0 = 2000\,\mathrm{G}$ as a function of MW frequency ω_{mw} for a σ^+-polarized MW field with an amplitude $B_{\mathrm{mw}} = 140\,\mathrm{mG}$. At $\omega_{\mathrm{mw}} = 5.609\,\mathrm{GHz}$ (dashed-dotted vertical line), the average of a_{12} and a_{13} equals a_{23}. If a σ^--polarized RF field resonant with the $|2\rangle$–$|3\rangle$ transition is applied at this point (dashed-dotted vertical line), the three scattering lengths can be made identically equal. (Lower panel) The two-body inelastic rate constants K_2 associated with a_{12}, a_{23} and a_{13}.

field of color superconductivity [1]. In this section, we describe how atomic systems in optical lattices can be engineered to have degrees of freedom in addition to the internal Zeeman state of the atom. To be specific, we suggest how a system with an additional pseudo-spin-1/2 degree of freedom can be realized by confining a three-component Fermi gas in the p-orbital band of an optical lattice. Superfluidity in a system with both color and spin degrees of freedom would provide an analogue of the single-flavor color superconducting phase that may occur in quark matter at intermediate densities.

Atoms localized on individual sites of an optical lattice can occupy either the lowest eigenstate of the potential at a given site (i.e. the s-orbital) or higher-lying eigenstates, such as the p_x, p_y or p_z orbitals. For a simple cubic lattice with equal lattice depths in each direction, the p_x, p_y and p_z orbitals are degenerate. Atoms occupying the p-orbital band of an optical lattice therefore have an orbital degree of freedom in addition to the degree of freedom associated with their internal state. Here, we will examine a case where atoms only occupy the p_x and p_y orbitals in a simple tetragonal lattice. We assume that the lattice depth and/or lattice constant in the z-direction is adjusted so that the p_z orbital has an energy higher than that of the p_x or p_y orbitals and is made energetically inaccessible. In this situation, atoms will be able to occupy either the p_x or p_y orbital and this two-state system will provide a pseudo-spin-1/2 degree of freedom in addition to the internal state of the atom.

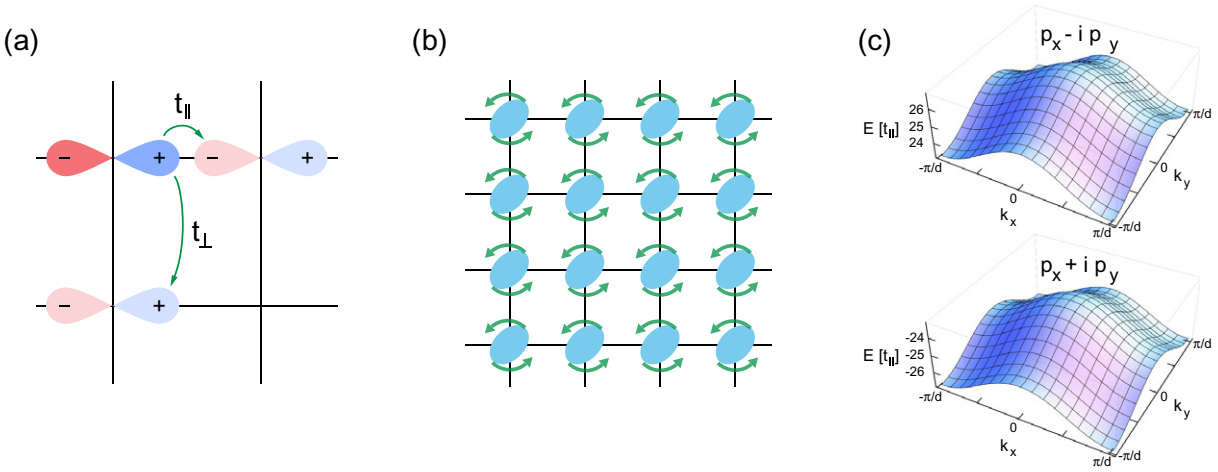

Figure 7. (a) Anisotropic tunneling in the $p_{x,y}$ band of an optical lattice. The matrix element $t_\parallel$ for tunneling parallel to the bond direction is significantly larger than $t_\perp$ associated with tunneling perpendicular to the bond direction. (b) To lift the degeneracy of the p_x and p_y orbitals and to make tunneling isotropic in the xy-plane, each lattice site can be rotated around its own center at angular frequency Ω. (c) The dispersion relation $E(k_x, k_y)$ for the $(p_x \pm \mathrm{i}p_y)$-bands when $\hbar\Omega = 25\, t_\parallel$ and $t_\perp = \frac{1}{10} t_\parallel$ in units of $t_\parallel$.

For identical lattice potentials in the x- and y-directions, the tight-binding Hamiltonian for a non-interacting three-component gas of fermions in the p_x/p_y-band is given by

$$H_{\mathrm{p_{x,y}}} = \sum_{i,\alpha}^{\sigma,\nu=x,y} t_{\sigma\nu}\left[c^\dagger_{i,p_\sigma,\alpha}\, c_{i+\nu,p_\sigma,\alpha} + \mathrm{h.c.}\right] + t_z \sum_{\langle mn\rangle,\alpha}^{\sigma=\uparrow,\downarrow}\left[c^\dagger_{m,p_\sigma,\alpha}\, c_{n,p_\sigma,\alpha} + \mathrm{h.c.}\right], \tag{8}$$

where $c^\dagger_{i,p_\sigma,\alpha}$ creates a particle at site i in orbital state p_σ with internal state $\alpha = 1, 2, 3$, $t_{\sigma\nu} = t_\parallel \delta_{\sigma\nu} + t_\perp(1 - \delta_{\sigma\nu})$ is an anisotropic tunneling matrix element for tunneling in the xy-plane, and t_z is the tunneling matrix element for hopping along the z-axis. The anisotropy of the matrix element $t_{\sigma\nu}$ accounts for the fact that the matrix element for tunneling in the direction parallel to the bond direction, $t_\parallel$, can significantly differ from the matrix element for tunneling perpendicular to the bond direction, $t_\perp$. These tunneling matrix elements, which are determined by wavefunction overlaps on adjacent sites, are depicted in figure 7(a). In general, $t_\parallel \gg t_\perp$. Due to the anisotropy of tunneling matrix elements for p_x and p_y orbitals, the Hamiltonian in equation (8) is explicitly *not* symmetric under SU(2) transformations of the p-orbital index although it is SU(3)-symmetric with respect to the color index. SU(2) $\otimes$ SU(3) symmetry can be realized by rotating the individual lattice sites about their own center, as we now discuss.

By rapidly modulating the position of the optical lattice in both the x- and y-directions, it is possible to create a square optical lattice for which the time-averaged potential at each lattice site has an elliptical constant energy contour in the xy-plane (see figure 7(b)). The relative phase and amplitude of the modulation in the x- and y-directions determine the orientation of the ellipse. The angle that the semi-major axis of the ellipse makes with the x-axis can be made to increase linearly in time so that each lattice site rotates around its own center at an angular frequency Ω. This technique was recently demonstrated by Gemelke *et al* [34]. Rotation causes

a coupling between the p_x and p_y orbitals on each individual lattice site described by [35]

$$H_L = \mathrm{i}\hbar\Omega \sum_{i,\alpha} \left[c^\dagger_{i,p_x,\alpha} c_{i,p_y,\alpha} - c^\dagger_{i,p_y,\alpha} c_{i,p_x,\alpha} \right]. \tag{9}$$

Rotating each lattice about its own center lifts the degeneracy of the p_x and p_y orbitals. The dispersion relation $E(k_x, k_y)$ for the tight-binding model given by $H_{\mathrm{p_{x,y}}} + H_L$ is shown in figure 7(c) for the parameters $\hbar\Omega = 25 t_\parallel$ and $t_\perp = \frac{1}{10} t_\parallel$. In the limit that $\Omega \gg t_\parallel$, the new eigenstates are $p_x \pm \mathrm{i} p_y$ orbitals, which are split in energy by $2\hbar\Omega$. The $p_x \pm \mathrm{i} p_y$ orbitals are azimuthally symmetric and, as a result, the tunneling matrix elements between $p_x \pm \mathrm{i} p_y$ orbitals on adjacent sites in the xy-plane are isotropic. In this limit, the system is described by an effective Hamiltonian with tunneling matrix elements between nearest neighbors in the xy-plane given by $t_{\mathrm{eff}} = \frac{1}{2}\left(t_\parallel + t_\perp\right)$,

$$H_{\mathrm{eff}} = t_{\mathrm{eff}} \sum_{\langle ij\rangle,\alpha}^{\sigma=\uparrow,\downarrow} \left[c^\dagger_{i,p_\sigma,\alpha}\, c_{j,p_\sigma,\alpha} + \mathrm{h.c.} \right] + t_z \sum_{\langle mn\rangle,\alpha}^{\sigma=\uparrow,\downarrow} \left[c^\dagger_{m,p_\sigma,\alpha}\, c_{n,p_\sigma,\alpha} + \mathrm{h.c.} \right]. \tag{10}$$

Here, the symbol $\uparrow$ ($\downarrow$) represents the $p_x + \mathrm{i} p_y$ ($p_x - \mathrm{i} p_y$) orbital, $\langle ij\rangle$ denotes that the sum is over nearest neighbors in the xy-plane and $\langle mn\rangle$ denotes that the sum is over nearest neighbors in the z-direction. In contrast to equation (8), the effective Hamiltonian H_{eff} is symmetric under SU(2) transformations of the orbital (pseudo-spin) index and SU(3) transformations of the internal state (color) index.

Finally, we have considered that fermions in different internal states can interact via an s-wave contact interaction potential $V(\mathbf{r} - \mathbf{r}') = \frac{4\pi\hbar^2 a_{\mathrm{t}}}{m} \delta(\mathbf{r} - \mathbf{r}')$. The Hamiltonian describing on-site interactions is

$$H_{\mathrm{int}} = \frac{U}{2} \sum_i \sum_{\alpha\neq\beta} \left[\sum_{\sigma,\sigma'} n_{i,p_\sigma,\alpha}\, n_{i,p_{\sigma'},\beta} + \sum_{\sigma\neq\sigma'} c^\dagger_{i,p_\sigma,\alpha} c^\dagger_{i,p_{\sigma'},\beta} c_{i,p_\sigma,\beta} c_{i,p_{\sigma'},\alpha} \right], \tag{11}$$

$$U = \frac{4\pi\hbar^2 a_{\mathrm{t}}}{m} \int \mathrm{d}^3\mathbf{r} \left| w_{p_x \pm \mathrm{i} p_y}(\mathbf{r}) \right|^4 = \frac{4\pi\hbar^2 a_{\mathrm{t}}}{m} \int \mathrm{d}^3\mathbf{r} \left| w_{p_x + \mathrm{i} p_y}(\mathbf{r}) \right|^2 \left| w_{p_x - \mathrm{i} p_y}(\mathbf{r}) \right|^2, \tag{12}$$

where $w_{p_x \pm \mathrm{i} p_y}$ are the Wannier wave functions for the $p_x \pm \mathrm{i} p_y$ orbitals. The first term accounts for on-site interactions between fermions in the same or different orbitals and the second term describes color exchange between unlike orbitals (or orbital exchange between unlike colors). To explicitly show the symmetry of the interaction Hamiltonian, we rewrite equation (11) in the form

$$H_{\mathrm{int}} = \frac{U}{2} \sum_i \sum_{\alpha,\beta} \sum_{\sigma,\sigma'} \left[n_{i,p_\sigma,\alpha}\, n_{i,p_{\sigma'},\beta} + c^\dagger_{i,p_\sigma,\alpha} c^\dagger_{i,p_{\sigma'},\beta} c_{i,p_\sigma,\beta} c_{i,p_{\sigma'},\alpha} - \delta_{p_\sigma p_{\sigma'}} n_{i,p_\sigma,\alpha} n_{i,p_{\sigma'},\beta} \right]. \tag{13}$$

This interaction Hamiltonian is invariant under SU(3) transformations of the color index. However, the last term breaks the SU(2) symmetry down to a U(1) symmetry. This symmetry-breaking term arises from the fact that the on-site interaction for a pair of fermions in unlike color states is different for the three symmetric triplet-orbital states. Specifically, the interaction energy for two atoms in identical orbital states is half that for a symmetric combination of $p_\uparrow$ and $p_\downarrow$ orbitals.

In future work, we will investigate the symmetry-breaking pattern and phase diagram for BCS superfluidity in this system, which has a $\mathrm{U}(1) \otimes \mathrm{SU}(3) \otimes \mathrm{U}(1)$ symmetry for the orbital,

color and overall phase. We will also investigate whether systems can be engineered that are symmetric under SU(2) ⊗ SU(3) ⊗ U(1) transformations when interactions are included. In this case, there would be several possible pairing patterns for the superfluid state analogous to the pairing patterns that occur for single-flavor color superconductivity (i.e. the color-spin locked, planar, polar and A-phases [36]). Such a system would offer the possibility of experimentally determining which pairing pattern is favored by nature in the presence of strong interactions and imbalanced populations, providing insights into the color superconducting phases thought to occur inside neutron stars.

Acknowledgments

We thank J Jain for valuable discussions about symmetry breaking. This work was supported by the Air Force Office of Scientific Research under grant no. FA9550-08-1-0069, the National Science Foundation under grant no. PHY10-11156 and the Army Research Office under grant no. W911NF-06-1-0398, which included partial funding from the DARPA OLE program.

References

[1] Alford M G, Schmitt A, Rajagopal K and Schäfer T 2008 Color superconductivity in dense quark matter *Rev. Mod. Phys.* **80** 1455–15
[2] Modawi A G K and Leggett A J 1997 Some properties of a spin-1 Fermi superfluid: application to spin-polarized Li-6 *J. Low Temp. Phys.* **109** 625–39
[3] Honerkamp C and Hofstetter W 2004 BCS pairing in Fermi systems with N different hyperfine states *Phys. Rev.* B **70** 094521
[4] Honerkamp C and Hofstetter W 2004 Ultracold fermions and the SU(N) Hubbard model *Phys. Rev. Lett.* **92** 170403
[5] He L, Jin M and Zhuang P 2006 Superfluidity in a three-flavor Fermi gas with SU(3) symmetry *Phys. Rev.* A **74** 033604
[6] Paananen T, Martikainen J P and Torma P 2006 Pairing in a three-component Fermi gas *Phys. Rev.* A **73**
[7] Paananen T, Törmä P and Martikainen J-P 2007 Coexistence and shell structures of several superfluids in trapped three-component fermi mixtures *Phys. Rev.* A **75** 023622
[8] Zhai H 2007 Superfluidity in three-species mixtures of Fermi gases across Feshbach resonances *Phys. Rev.* A **75**
[9] Catelani G and Yuzbashyan E A 2008 Phase diagram, extended domain walls, and soft collective modes in a three-component fermionic superfluid *Phys. Rev.* A **78** 033615
[10] Bedaque P F and D'Incao J P 2009 Superfluid phases of the three-species fermion gas *Ann. Phys.* **324** 1763–8
[11] Ozawa T and Baym G 2010 Population imbalance and pairing in the BCS–BEC crossover of three-component ultracold fermions *Phys. Rev.* A **82** 063615
[12] Cherng R W, Refael G and Demler E 2007 Superfluidity and magnetism in multicomponent ultracold fermions *Phys. Rev. Lett.* **99**
[13] Rapp A, Zarand G, Honerkamp C and Hofstetter W 2007 Color superfluidity and 'Baryon' formation in ultracold fermions *Phys. Rev. Lett.* **98**
[14] Rapp A, Hofstetter W and Zarand G 2008 Trionic phase of ultracold fermions in an optical lattice: A variational study *Phys. Rev.* B **77** 144520
[15] Bartenstein M *et al* 2005 Precise determination of Li-6 cold collision parameters by radio-frequency spectroscopy on weakly bound molecules *Phys. Rev. Lett.* **94** 103201
[16] Griffiths D 2004 *Introduction to Elementary Particles* 2nd edn (New York: Wiley-VCH)

[17] Hatsuda T, Tachibana M, Yamamoto N and Baym G 2006 New critical point induced by the axial anomaly in dense qcd *Phys. Rev. Lett.* **97** 122001
[18] Yamamoto N, Tachibana M, Hatsuda T and Baym G 2007 Phase structure, collective modes, and the axial anomaly in dense qcd *Phys. Rev.* D **76** 074001
[19] Williams J R, Hazlett E L, Huckans J H, Stites R W, Zhang Y and O'Hara K M 2009 Evidence for an excited-state Efimov trimer in a three-component Fermi gas *Phys. Rev. Lett.* **103** 130404
[20] Petrov D S, Salomon C and Shlyapnikov G V 2004 Weakly bound dimers of fermionic atoms *Phys. Rev. Lett.* **93** 090404
[21] Braaten E and Hammer H W 2007 Efimov physics in cold atoms *Ann. Phys.* **322** 120–63
[22] Hofstetter W, Cirac J I, Zoller P, Demler E and Lukin M D 2002 High-temperature superfluidity of fermionic atoms in optical lattices *Phys. Rev. Lett.* **89** 220407
[23] Staudt R, Dzierzawa M and Muramatsu A 2000 Phase diagram of the three-dimensional Hubbard model at half filling *Eur. Phys. J.* B **17** 411–5
[24] Blakie P B and Bezett A 2005 Adiabatic cooling of fermions in an optical lattice *Phys. Rev.* A **71**
[25] Ketterle W and Van Druten N J 1996 Evaporative cooling of trapped atoms *Adv. At. Mol. Opt. Phys.* **37** 181–236
[26] O'Hara K M 2000 Optical trapping and evaporative cooling of fermionic atoms *PhD Thesis* Duke University
[27] Kantian A, Dalmonte M, Diehl S, Hofstetter W, Zoller P and Daley A J 2009 Atomic color superfluid via three-body loss *Phys. Rev. Lett.* **103**
[28] Titvinidze I, Privitera A, Chang S-Y, Diehl S, Baranov M A, Daley A and Hofstetter W 2011 Magnetism and domain formation in SU(3)-symmetric multi-species Fermi mixtures *New J. Phys.* **13** 035013
[29] Moerdijk A J, Verhaar B J and Nagtegaal T M 1996 Collisions of dressed ground-state atoms *Phys. Rev.* A **53** 4343–51
[30] Hanna T M, Tiesinga E and Julienne P S 2010 Creation and manipulation of Feshbach resonances with radiofrequency radiation *New J. Phys.* **12**
[31] Kaufman A M, Anderson R P, Hanna T M, Tiesinga E, Julienne P S and Hall D S 2009 Radio-frequency dressing of multiple Feshbach resonances *Phys. Rev.* A **80** 050701
[32] Zhang P, Naidon P and Ueda M 2009 Independent control of scattering lengths in multicomponent quantum gases 2009 *Phys. Rev. Lett.* **103** 133202
[33] Tscherbul T V, Calarco T, Lesanovsky I, Krems R V, Dalgarno A and Schmiedmayer J 2010 rf-field-induced Feshbach resonances *Phys. Rev.* A **81** 050701
[34] Gemelke N, Sarajlic E and Chu S 2010 Rotating few-body atomic systems in the fractional quantum Hall regime arXiv:1007.2677v1
[35] Wu C 2008 Orbital analogue of the quantum anomalous hall effect in p-band systems *Phys. Rev. Lett.* **101** 186807
[36] Schmitt A 2005 Ground state in a spin-one color superconductor *Phys. Rev.* D **71** 054016